

## Article

# Structural Phase Transition in $(\text{NH}_4)_3\text{GeF}_7$ —Raman Spectroscopy Data

Yulia Gerasimova <sup>1,2</sup>, Natalia Laptash <sup>3</sup>, Alexander Krylov <sup>1,\*</sup> , Vita Vonog <sup>2</sup> and Alexander Vtyurin <sup>1,2</sup> <sup>1</sup> Kirensky Institute of Physics, Federal Research Center KSC SB RAS, 660036 Krasnoyarsk, Russia; jul@iph.krasn.ru (Y.G.); vtyurin@iph.krasn.ru (A.V.)<sup>2</sup> Siberian Federal University, 660041 Krasnoyarsk, Russia; vvonog@sfu-kras.ru<sup>3</sup> Institute of Chemistry, Far Eastern Branch of RAS, 690022 Vladivostok, Russia; laptash@ich.dvo.ru

\* Correspondence: shusy@iph.krasn.ru

**Abstract:** We obtained Raman spectra of  $(\text{NH}_4)_3\text{GeF}_7$  crystals with a wide range of frequencies (10–3400  $\text{cm}^{-1}$ ) and temperatures (8–300 K), including phase transition, which was accompanied by a symmetry increase with a temperature decrease. The internal vibrations of the  $\text{GeF}_6^{2-}$  group were classified by the positional symmetry method. Considerable transformations of the Raman spectra were observed at the lower frequency range of lattice vibrations and the ranges of the internal vibrations of the ammonium ions. In contrast, the internal modes of the  $\text{GeF}_6^{2-}$  groups changed only slightly due to their resonance splitting in the multiplied unit cell, which agreed well with the proposed phase transition mechanism induced by ammonium group ordering.

**Keywords:** fluorides; Raman spectra; lattice disordering



**Citation:** Gerasimova, Y.; Laptash, N.; Krylov, A.; Vonog, V.; Vtyurin, A. Structural Phase Transition in  $(\text{NH}_4)_3\text{GeF}_7$ —Raman Spectroscopy Data. *Crystals* **2021**, *11*, 506. <https://doi.org/10.3390/cryst11050506>

Academic Editor: Sergey V. Makarov

Received: 26 March 2021

Accepted: 30 April 2021

Published: 3 May 2021

**Publisher's Note:** MDPI stays neutral with regard to jurisdictional claims in published maps and institutional affiliations.



**Copyright:** © 2021 by the authors. Licensee MDPI, Basel, Switzerland. This article is an open access article distributed under the terms and conditions of the Creative Commons Attribution (CC BY) license (<https://creativecommons.org/licenses/by/4.0/>).

## 1. Introduction

Germanium is one of the purest semiconductors that have been made. Germanium is used to make light emitting diodes (LEDs), optical fibers, and solar cells. Nanowires are one of the most recent usages, and germanium is a promising anode material for lithium-ion batteries (LIBs) [1]. New types of Ge-based materials with different structural dimensions and the controlled formation of microstructures are leading to a reformation in the field of LIBs [2] and dual-ion batteries (DIBs) [3] as well as in sodium- and potassium-ion batteries (SIBs and PIBs) [4]. Chemical etching by an acid mixture of HF and  $\text{HNO}_3$  vapors of Si/Ge nanowire-grown silicon wafers activates or enhances photoluminescence of materials in the near-infrared region.

The results indicated that the treatment induces significant changes in the wafer surface [5]. Following a similar procedure, the Ge wafer was transformed to ammonium germanium fluoride  $(\text{NH}_4)_2\text{GeF}_6$  [6]. The compound is thermodynamically very stable [7]. Its double salt  $(\text{NH}_4)_2\text{MeF}_6 \cdot \text{NH}_4\text{F} = (\text{NH}_4)_3\text{GeF}_7 = (\text{NH}_4)_3[\text{GeF}_6]\text{F}$  formed by the fluorination of elemental germanium with ammonium hydrogen difluoride ( $\text{NH}_4\text{HF}_2$ ) was no less stable [8,9]. The interaction of germanium oxide ( $\text{GeO}_2$ ) with  $\text{NH}_4\text{HF}_2$  proceeds with an exo effect with the formation of this salt [10].

Ammonium heptafluoride germanate,  $(\text{NH}_4)_3\text{GeF}_7$ , belongs to a series of isomorphic ammonium fluoride double salts  $(\text{NH}_4)_2\text{MF}_6 \cdot \text{NH}_4\text{F} = (\text{NH}_4)_3\text{MF}_7 = (\text{NH}_4)_3[\text{MF}_6]\text{F}$  (M = Si, Ge, Sn, Ti), the structures of which were recently refined [11–14], and their optical and thermodynamic properties have been studied [15–19]. Unusual phase transitions were found in the case of Ge and Ti salts, which included an increase in symmetry with a decreasing temperature. The room temperature space group  $P4/m\bar{b}m$  of  $(\text{NH}_4)_3\text{GeF}_7$  was different from  $P4/m\bar{m}c$  of  $(\text{NH}_4)_3\text{TiF}_7$  [12,13]. A sequence of phase transitions  $P4/m\bar{b}m$  ( $T_1 = 279.4$  K)  $\leftrightarrow$   $Pb\bar{a}m$  ( $T_2 = 270$  K)  $\leftrightarrow$   $P2_1/c$  ( $T_3 = 227$  K)  $\leftrightarrow$   $Pa-3$  was found in  $(\text{NH}_4)_3\text{GeF}_7$  [12]. The structures of the initial and final phases are shown in Figure 1 according to the data of Mel'nikova et al. [12].

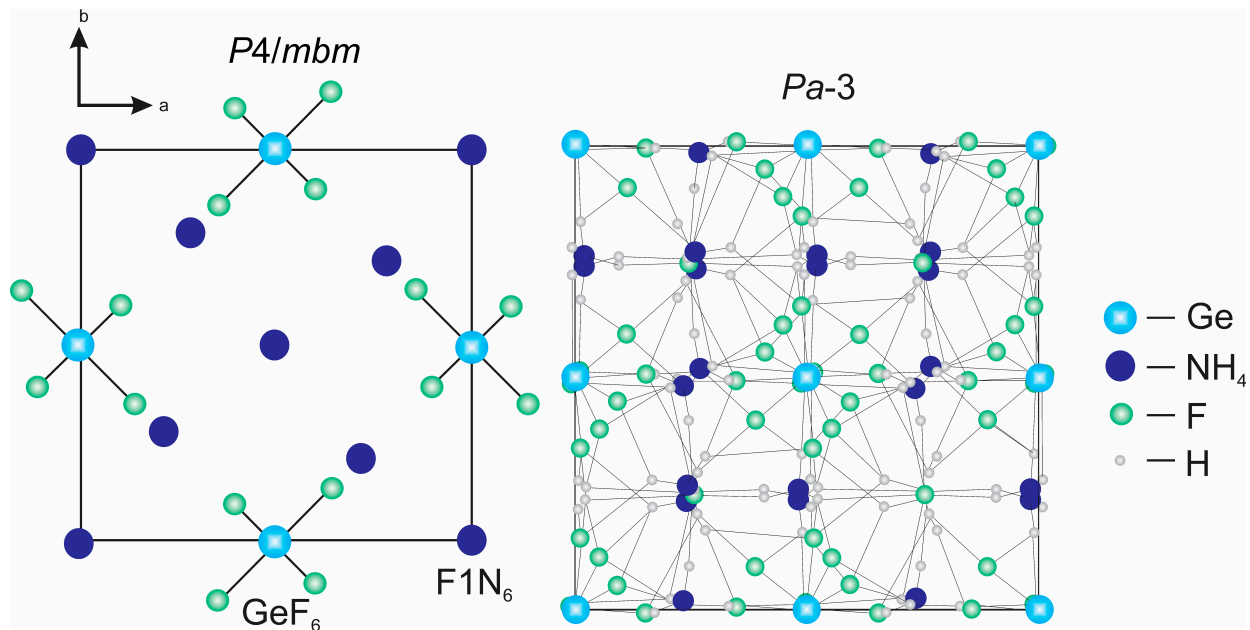


**Figure 1.** Structures of the room temperature  $P4/mbm$  and final  $Pa-3$  phases for  $(\text{NH}_4)_3\text{GeF}_7$  crystals according to previous data [12]. The hydrogen ions in the high-temperature phase were not localized and are not shown due to their disordering.

Detailed calorimetric investigations showed that the transitions  $P4/mbm \leftrightarrow Pbam \leftrightarrow P2_1/c$  are second-order and were induced by ammonium group ordering when cooling [16]. The reconstructive transition between the monoclinic  $P2_1/c$  and cubic  $Pa-3$  phases at 227 K is a pronounced first-order transformation with a significant contribution of latent heat to the total enthalpy change (~90%). The corresponding entropy change (12.5 J/mol K) turned out to be significantly less than that found in the related  $(\text{NH}_4)_3\text{TiF}_7$  (22.7 J/mol K) during the reconstructive transition  $P4/mnc \leftrightarrow Pa-3$  [13].

The observed difference in entropies during the transition to the same low-temperature phase was associated with a significant difference in the degree of disordering of structural elements in the monoclinic  $P2_1/c$  and tetragonal  $P4/mnc$  phases of germanate and titanate crystals, respectively [12,13]. We recently reported Raman studies of this family's crystals, including  $(\text{NH}_4)_3\text{GeF}_7$  [20]; however, some discrepancies between the spectral and calorimetric data for this complex prompted us to study this compound in more detail, which we present in this work.

## 2. Materials and Methods

The synthesis and crystal growth of  $(\text{NH}_4)_3\text{GeF}_7$  for spectral investigations was performed from fluoride aqueous solution as described in more detail in [12,16].

The Raman spectra of  $(\text{NH}_4)_3\text{GeF}_7$  were studied in the temperature range from 8 to 300 K and obtained in backscattering geometry using a Horiba Jobin Yvon T64000 (Horiba, Gières, France) triple Raman spectrometer operating in the dispersion subtraction mode and detected with a CCD matrix cooled with liquid nitrogen. The spectral resolution for the recorded Raman spectra was about  $2 \text{ cm}^{-1}$ . A Lxel 95-L (Cambridge Lasers Laboratorie, Fremont, CA, USA) single-mode krypton laser (647.1 nm and 15 mW at the sample) was used as an excitation source.

Low-temperature experiments were performed using an ARS CS204-X1.SS (Advanced Research Systems, USA) closed-loop helium cryostat with a LakeShore 340 temperature controller. The temperature was controlled using a LakeShore DT-670SD1.4L (LakeShore, USA) calibrated silicon diode. Spectroscopic measurements were performed in the subtractive dispersion mode, which attained a low-wavenumber limit of  $10 \text{ cm}^{-1}$  in the present setup. The deformation of the low-wavenumber spectral edge by an optical slit, which

sometimes smears the true features of low-wavenumber spectra, was carefully eliminated by rigorous optical alignment.

The temperature measurements were carried out in the dynamic regime by varying the sample temperature. The rate of temperature variation was 0.6 K/min. The uncertainty of the measured temperature for a given rate can be estimated as the difference between adjacent measurements and was  $\pm 0.45$  K in one spectrum measurement. The overall time for a single spectrum accumulation was within 45 s. The spectra were acquired with a temperature step of 0.1 K. This measurement protocol was reported in [21].

### 3. Results

Figure 2 shows the Raman intensity maps for internal modes of the  $\text{GeF}_6^{2-}$  octahedral group.

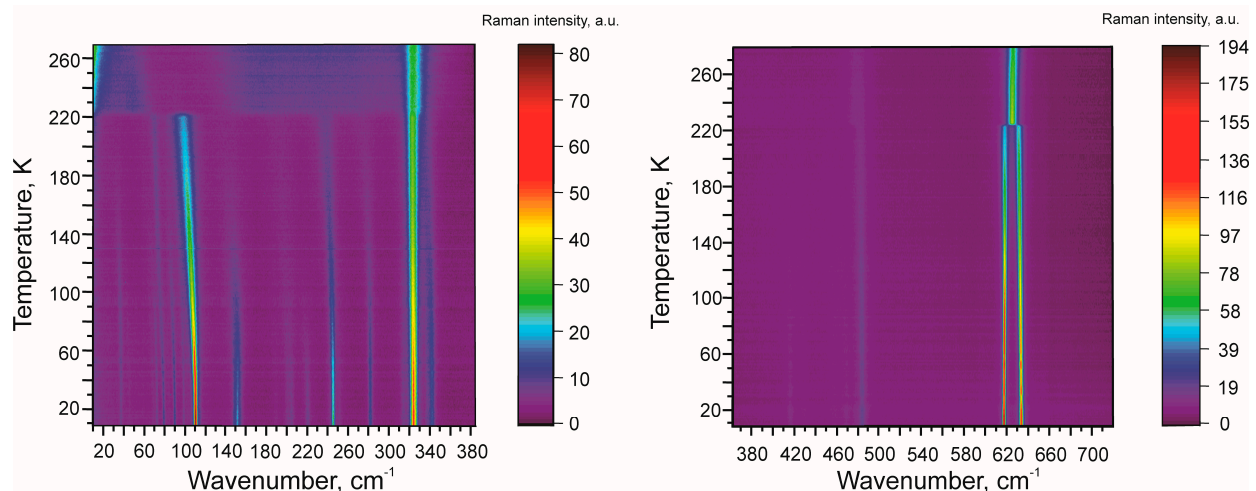


Figure 2. Raman spectra maps for  $(\text{NH}_4)_3\text{GeF}_7$ .

The internal vibrations of the  $\text{GeF}_6^{2-}$  group were classified by the positional symmetry method [22]. The symmetry of the  $(\text{NH}_4)_3\text{GeF}_7$  crystal is  $D_{4h}$  ( $P4/mbm$ ,  $Z = 2$ ), the symmetry of the free  $\text{GeF}_6^{2-}$  ion is  $O_h$ , and the symmetry of its position in the crystal is  $D_2$  [12], where  $Z$  is the number of formula units for a single unit cell. The vibrational representation of the Raman active modes for the free ion is  $\Gamma = A_{1g} + E_g + F_{2g}$ . The correlation diagram of the internal vibrations of the  $\text{GeF}_6^{2-}$  ion for the  $P4/mbm$  ( $D_{4h}$ ) and  $Pa-3$  ( $T_h$ ) phases is shown in Figure 3.

The symmetry of the position of the ion in the  $D_{2h}$  lattice is lower than its own symmetry  $O_h$ , which results in a splitting of the degenerate vibrations of the free ion  $E \rightarrow A + B$  and  $F \rightarrow A + 2B$ . The presence of two ions in the cell caused the Davydov splitting of each type of symmetry of the positional group  $D_{2h}$  into two components (Figure 3).

On the presented maps of the Raman intensity distribution above 223 K, two intense vibrations at 625 and 325  $\text{cm}^{-1}$  are well visualized, and one more vibration near 470  $\text{cm}^{-1}$  has a weak intensity, which corresponds to the correlation diagram where there are two  $A_{1g}$  lines attributed to the  $\nu_1$  and  $\nu_2$  modes. According to [22], the frequency of the  $\nu_1$  mode for the free ion is 624  $\text{cm}^{-1}$ , and for the  $\nu_2$  mode, it is 471  $\text{cm}^{-1}$ .

Therefore, in the Raman spectra of the crystal, the 625  $\text{cm}^{-1}$  line corresponds to a full symmetric stretching mode  $\nu_1$ , and the peak at 470  $\text{cm}^{-1}$  is the internal bending vibrations of the  $\nu_2$  type of the  $\text{GeF}_6^{2-}$  groups, while  $A_{2g}$  and  $B_{2g}$  are Raman inactive. The vibration frequency  $\nu_5$  of a free ion is 335  $\text{cm}^{-1}$ ; in the crystal spectrum, a doublet in the region of 325  $\text{cm}^{-1}$  corresponds to this three-fold degenerate vibration. As in titanium heptafluoride, here in the  $P4/mbm$  phase, we observed a high intensity of the Rayleigh wing.

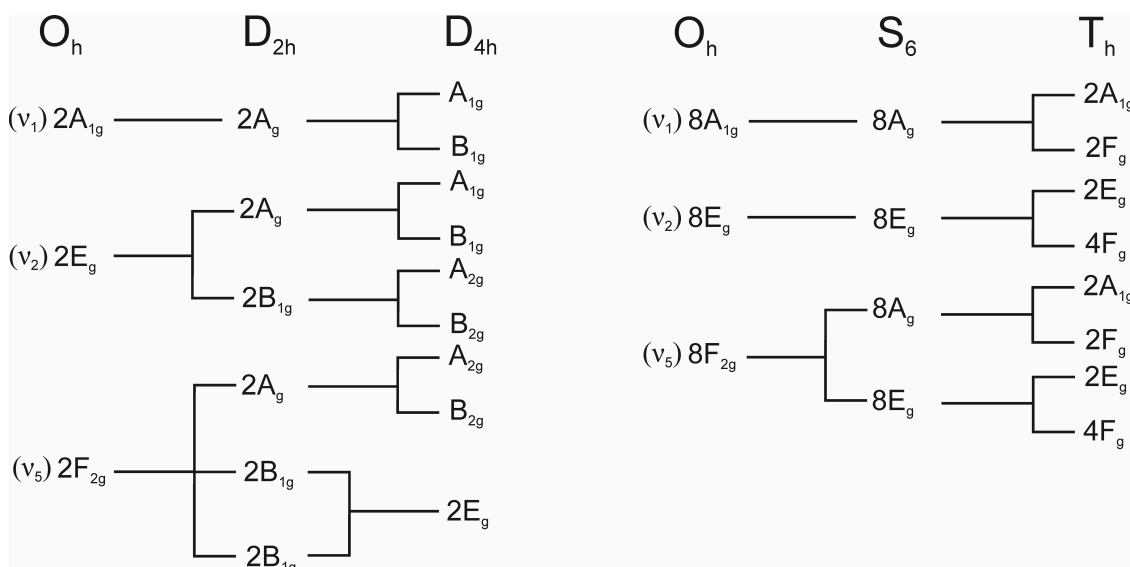


Figure 3. Correlation diagram for the internal modes of  $\text{GeF}_6^{2-}$  ions.

Let us consider the changes in the spectrum in the region of the octahedron vibrations with cooling (Figure 2). In the low-temperature phase, the crystal has a space group  $Pa-3$ ; its unit cell is increased and now contains eight formula units ( $Z = 8$ ) [12]. When approaching the phase transition, no anomalies were observed in the spectrum, and the phase transition at 223 K was accompanied by line splitting at  $625 \text{ cm}^{-1}$ . A further cooling led to the appearance of many narrow spectral lines (Figure 2), indicating a significant change in the structure.

According to the correlation diagram (Figure 3), the  $\text{GeF}_6^{2-}$  ion in the vector representation of the  $S_6$  positional group had the following features. Vector representations in group  $S_6$  were  $A_g + E_g$ . The doubly degenerate vibration E correlated with the doubled twice degenerate and quadruple three times degenerate vibrations of the  $T_h$  group. As a result, we obtained the presentation  $\Gamma = 4A_{1g} + 4E_g + 12F_g$ , for the Raman active internal modes of these ions; thus, in the low-temperature phase, we expected the appearance of 20 lines in the corresponding region of the Raman spectra.

However, in the experimental spectra, most of the new lines belong to the low-frequency range of the external lattice vibrations, while these 20 predicted internal modes are not shown in the spectra. This absence of the expected lines in this region may be due to rather small distortions of the rigid  $\text{GeF}_6^{2-}$  octahedra below the transition point while the splitting of the  $625 \text{ cm}^{-1}$  line should be attributed to dynamical Davydov interactions in a larger unit cell of the new crystal structure.

Below 223 K, a new intense line appeared at  $115 \text{ cm}^{-1}$  in the lower frequency range of the lattice modes that correspond to the translational intramolecular vibrations of ammonium ions (Figure 2). The appearance of a very similar line at  $97 \text{ cm}^{-1}$  was observed below the reconstructive phase transition in the  $(\text{NH}_4)_3\text{TiF}_7$  crystal where it was ascribed to the shortening of the distances between free fluorine ions and ammonium groups [20]. This shortening of these distances with distortions of the fluorine ion coordination environment below the transition point was reported earlier in [12].

Therefore, we attribute this  $115 \text{ cm}^{-1}$  line to the appearance of stronger bonds between free fluorine ions and ammonium groups, while the higher frequency is connected with a larger size of Ge ions as compared with Ti ones. In the region of bending vibrations of ammonium groups, cooling below the PT point results in the appearance of narrow and intense peaks in place of broad low-intensity bands. Intense but broader peaks also appear in the region of stretching vibrations (Figure 4).

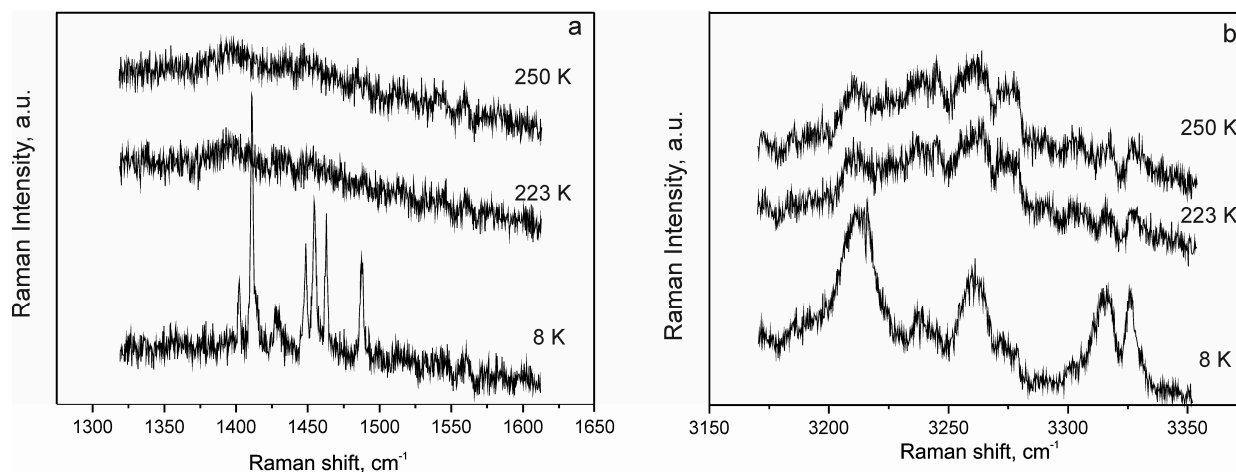


**Figure 4.** Temperature transformations of the Raman spectra in the ranges of bending (a) and stretching (b) modes of ammonium groups.

According to [12], the stepwise ordering of ammonium tetrahedra, disordered in the initial phase, occurs as a result of phase transitions in  $(\text{NH}_4)_3\text{GeF}_7$ , which is accompanied by significant changes in entropy as well as rotations of the octahedra, which leads to a decrease in interatomic distances and the formation of stronger  $\text{N-H} \cdots \text{F}$  hydrogen bonds. Thus, the main reason for the observed structural transformation is hydrogen bonds strengthening under cooling. Observed modifications of the spectra in the range of the ammonium internal vibrations are in complete agreement with these ordering processes.

#### 4. Conclusions

Single crystals of double germanium fluoride  $(\text{NH}_4)_3\text{GeF}_7$  were studied using Raman scattering in a wide temperature and frequency range, with particular attention to the unusual sequence of phase transitions, which was found recently. The studied crystals, like titanium heptafluoride, undergo a phase transition with an increase in symmetry, but, as was established, only from the tetragonal phase to the cubic one. A wide Rayleigh wing was found in the  $P4/mbm$  phase, which disappeared closer to the transition point and, thus, provides evidence of disordering in this phase.

We confirmed that the ordering processes of ammonium groups were the main mechanism of the structural reconstructions  $P4/mbm \rightarrow Pa-3$ , which was demonstrated in the spectra of  $\text{NH}_4^+$  internal vibrations. Lower frequency external modes transformed considerably as well, while the internal vibrations of the octahedral group  $\text{GeF}_6^{2-}$  changed only slightly. The splitting of the  $625 \text{ cm}^{-1}$  line into a doublet, which was attributed to the dynamical resonance interaction of internal modes in the larger unit cell, was the most impressive change in this region.

**Author Contributions:** Conceptualization, Y.G., A.K., and A.V.; methodology, N.L., A.K. and Y.G.; software, Y.G., A.K.; validation, Y.G. and A.V.; investigation, Y.G., A.K., and N.L.; data curation, Y.G. and V.V.; writing—original draft preparation, N.L., V.V., and Y.G. writing—review and editing, Y.G., N.L., V.V., A.K. and A.V.; visualization, Y.G., and A.K.; supervision, Y.G. and A.V. All authors have read and agreed to the published version of the manuscript.

**Funding:** This research was partially funded by RFBR and DFG, project No. 21-52-12018.

**Institutional Review Board Statement:** Not applicable.

**Informed Consent Statement:** Not applicable.

**Data Availability Statement:** Raw data of this paper will be available from corresponding author, A.K., on a reasonable request.

**Conflicts of Interest:** The authors declare no conflict of interest.

## References

1. Hao, J.; Yang, Y.; Zhao, J.P.; Liu, X.S.; Endres, F.; Chi, C.X.; Wang, B.S.; Liu, X.X.; Li, Y. Ionic liquid electrodeposition of strain-released Germanium nanowires as stable anodes for lithium ion batteries. *Nanoscale* **2017**, *9*, 8481–8488. [[CrossRef](#)] [[PubMed](#)]
2. Qin, J.W.; Cao, M.H. Multidimensional germanium-based materials as anodes for Lithium-ion batteries. *Chem. Asian J.* **2016**, *20*, 1169–1181. [[CrossRef](#)] [[PubMed](#)]
3. Zhou, J.; Zhou, Y.; Zhang, X.; Cheng, L.W.; Qian, M.M.; Wei, W.; Wang, H. Germanium-based high-performance dual-ion batteries. *Nanoscale* **2020**, *12*, 79–84. [[CrossRef](#)] [[PubMed](#)]
4. Loaiza, L.C.; Monconduit, L.; Seznec, V. Si and Ge-based anode materials for Li-, Na-, and K-ion batteries: A perspective from structure to electrochemical mechanism. *Small* **2020**, *16*, e1905260. [[CrossRef](#)]
5. Kalem, S.; Werner, P.; Talalaev, V. Near-IR photoluminescence from Si/Ge nanowire-grown silicon wafers: Effect of HF treatment. *Appl. Phys. A* **2013**, *112*, 561–567. [[CrossRef](#)]
6. Kalem, S.; Arthursson, Ö.; Romandic, I. Formation of germanates on germanium by chemical vapor treatment. *Thin. Solid Films* **2010**, *518*, 2377–2380. [[CrossRef](#)]
7. Yota, J.; Burrows, V.A. An infrared-study of thin-film formation on Si and Ge surfaces treated with aqueous  $\text{NH}_4\text{F}$  and HF. *J. Appl. Phys.* **1991**, *69*, 7369–7371. [[CrossRef](#)]
8. Plitzko, C.; Meyer, G. Crystal structure of triammonium heptafluorogermanate  $(\text{NH}_4)_3\text{GeF}_7$ . *Z. Kristallogr.* **1998**, *213*, 475. [[CrossRef](#)]
9. Meyer, G. The Oxidation of metals with Liebig acids. *Z. Anorg. Allg. Chem.* **2008**, *634*, 201–222. [[CrossRef](#)]
10. D'yachenko, A.N.; Kraidenko, R.I. Fluorination of germanium concentrates with ammonium fluorides. *Russ. J. Appl. Chem.* **2008**, *81*, 952–955. [[CrossRef](#)]
11. Mel'nikova, S.V.; Molokeev, M.S.; Laptash, N.M.; Pogoreltsev, E.I.; Misyul, S.V.; Flerov, I.N. Sequence of phase transitions in  $(\text{NH}_4)_3\text{SiF}_7$ . *Dalton Trans.* **2017**, *46*, 2609–2617. [[CrossRef](#)]
12. Mel'nikova, S.V.; Molokeev, M.S.; Laptash, N.M.; Misyul, S.V. A non-typical sequence of phase transitions in  $(\text{NH}_4)_3\text{GeF}_7$ : Optical and structural characterization. *Dalton Trans.* **2016**, *45*, 5321–5327. [[CrossRef](#)]
13. Molokeev, M.; Misyul, S.V.; Flerov, I.N.; Laptash, N.M. Reconstructive phase transition in  $(\text{NH}_4)_3\text{TiF}_7$  accompanied by the ordering of  $\text{TiF}_6$  octahedra. *Acta. Cryst.* **2014**, *B70*, 924–931. [[CrossRef](#)]
14. Flerov, I.N.; Molokeev, M.S.; Laptash, N.M.; Udovenko, A.A.; Pogoreltsev, E.I.; Mel'nikova, S.V.; Misyul, S.V. Structural transformation between two cubic phases of  $(\text{NH}_4)_3\text{SnF}_7$ . *J. Fluorine Chem.* **2015**, *178*, 86–92. [[CrossRef](#)]
15. Pogoreltsev, E.I.; Bogdanov, E.V.; Kartashev, A.V.; Molokeev, M.S.; Flerov, I.N.; Laptash, N.M. Thermal properties of  $(\text{NH}_4)_2\text{MeF}_6 \cdot \text{NH}_4\text{F}$  (Me: Ti, Sn) crystals undergoing transformation between two cubic phases. *Ferroelectrics* **2016**, *501*, 20–25. [[CrossRef](#)]
16. Bogdanov, E.V.; Kartashev, A.V.; Pogoreltsev, E.I.; Gorev, M.V.; Laptash, N.M.; Flerov, I.N. Anomalous behaviour of thermodynamic properties at successive phase transitions in  $(\text{NH}_4)_3\text{GeF}_7$ . *J. Solid State Chem.* **2017**, *256*, 162–167. [[CrossRef](#)]
17. Mel'nikova, S.V.; Pogoreltsev, E.I.; Flerov, I.N.; Laptash, N.M. Unusual sequence of phase transitions in  $(\text{NH}_4)_3\text{TiF}_7$  detected by optic and calorimetric studies. *J. Fluorine Chem.* **2014**, *165*, 14–19. [[CrossRef](#)]
18. Pogoreltsev, E.I.; Flerov, I.N.; Kartashev, A.V.; Bogdanov, E.V.; Laptash, N.M. Heat capacity, entropy, dielectric properties and T-p phase diagram of  $(\text{NH}_4)_3\text{TiF}_7$ . *J. Fluorine Chem.* **2014**, *168*, 247–250. [[CrossRef](#)]
19. Kartashev, A.V.; Gorev, M.V.; Bogdanov, E.V.; Flerov, I.N.; Laptash, N.M. Thermal properties and phase transition in the fluoride,  $(\text{NH}_4)_3\text{SnF}_7$ . *J. Solid State Chem.* **2016**, *237*, 269–273. [[CrossRef](#)]
20. Gerasimova, Y.V.; Krylov, A.S.; Vtyurin, A.N.; Laptash, N.M.; Krylova, S.N. Ferroelastic phase transition in the family of double fluoride crystals by Raman spectroscopy. *Ferroelectrics* **2020**, *568*, 185–190. [[CrossRef](#)]
21. Krylov, A.S.; Kolesnikova, E.M.; Isaenko, L.I.; Krylova, S.N.; Vtyurin, A.N. Measurement of Raman-scattering spectra of  $\text{Rb}_2\text{KMoO}_3\text{F}_3$  crystal: Evidence for controllable disorder in the lattice structure. *Cryst. Growth Des.* **2014**, *14*, 923–927. [[CrossRef](#)]
22. Nakamoto, K. *Infrared and Raman Spectra of Inorganic and Coordination Compounds*, 6th ed.; Wiley: New York, NY, USA, 2009; p. 419.